

Single-mode phonon transmission in symmetry broken carbon nanotubes

Jian Wang¹ and Jian-Sheng Wang²

¹College of Physical Science and Technology,
Yangzhou University, Yangzhou 225002, P. R. China

²Center for Computational Science and Engineering and Department of Physics,
National University of Singapore, Singapore 117542, Republic of Singapore

(Dated: 25 July 2008)

Abstract

Normal mode phonon transmissions are studied in carbon nanotubes with the presence of Stone-Wales (SW) defect, using a mode-matching method and through the analysis of symmetry. The calculation shows that the transmission for low group velocity acoustic phonons is evidently reduced at high frequency range, and that this SW defect induced symmetry breaking strongly inhibits the transmission of long wave optical phonons in carbon nanotubes. The characteristic features of transmission for each phonon mode depend on the symmetry. These findings suggest that the local heating in the defective nanotubes may be contributed mainly from the low group velocity acoustic phonons and optical phonons near the Γ -point.

Carbon nanotubes (CNTs) are uniquely symmetric^{1,2,3} quasi-one-dimensional structures with remarkable electrical, mechanical, and thermal properties for various engineering applications.^{2,4,5,6,7} However, such symmetries for perfect carbon nanotubes are usually broken⁵, either for the purposes of engineering application such as the junction structure, or due to the technical flaws during the process of synthesis such as the Stone-Wales (SW) defects. When the symmetry of structures is broken, the equation of motion that underlines the physical properties of material does not respect the symmetry anymore.⁸ Therefore, such symmetry breaking in nanotubes is important for deep insight into both physical properties and transport behavior. The total transmissions for all possible normal mode phonons at a given frequency have been first studied using the nonequilibrium Green's function method (NEGF).⁹ Of particular interest in this letter is the single-mode phonon transmission of CNTs in the presence of the SW defect, which is known as the explicit symmetry breaking mechanism. Understanding single-mode phonon transmission in the symmetry broken nanotubes is not only fundamental to addressing the heat dissipation in nanodevices which challenges the current electronic miniaturization and the thermal transport in carbon nanotubes,^{4,5,6,7} but also relevant to the phonon control problem in the emerging phononic devices.^{10,11,12} This letter aims to study the behavior of single-mode phonon transmission in the symmetry broken nanotubes with the SW defect through the analysis of its symmetrical property. We first introduce the mode-matching method^{13,14,15} used in our calculations. Then the phonon dispersion of the single-walled achiral carbon nanotube (11;0) is calculated from the force constants derived from the second-generation Brenner potential.¹⁷ Each branch of normal mode phonon is further analyzed within the full symmetry of line group theory. Finally we present the calculated results of single-mode phonon transmission in the symmetry broken CNT (11;0) in the presence of the SW defect, using the mode-matching method.

The NEGF^{9,15,16,18} has been employed to calculate phonon transmission coefficient which is the sum of all the normal modes from the leads. It is in principle at least applicable to both the elastic and nonlinear scattering regime.¹⁵ However, it is difficult to analyze the contribution from each mode, respectively. The mode-matching method^{13,14,15} serves as another equivalent way to calculate the transmission coefficient in the ballistic limit. In comparison with NEGF, the most prominent advantage of the mode-matching method is that the single mode phonon transmission can be obtained from this method explicitly.

But the mode-matching method is valid only in the elastic regime, where the anharmonic scattering is neglected. In the low-dimensional carbon nanotubes, anharmonic scattering does not play an important role in thermal transport below room temperature and thermal transport is found almost ballistic through the experiments.^{6,7} The dominant scattering mechanism is elastic due to topological defects or impurities in CNTs at low temperatures. Therefore, we focus our discussion on the elastic regime. The mode-matching is the exact method of calculating the single mode phonon transmission for the elastic scattering.

We assume that one normal mode^{13,14,15} $\alpha_{lm}(\omega; \mathbf{q}) = \mathbf{e}_n e^{i(\mathbf{q} \cdot \mathbf{R}_l - \omega t)}$ is incident from the left lead, where each eigenvector \mathbf{e}_n satisfies the dynamic equation of motion¹⁵ $D \mathbf{e}_n = \omega^2 \mathbf{e}_n$. Here D is the dynamic matrix for the unit cell on the perfect lead, l denotes the atom in the l unit cell, \mathbf{R}_l denotes the position for the l unit cell, and n refers to the polarized phonon branch. Angular frequency is denoted as ω , wavevector as \mathbf{q} . Due to the defect scattering in the central region, the solution for the left/right perfect leads can be written as¹⁵

$$u_1^L = \alpha_{lm}(\omega; \mathbf{q}) + \sum_{n^0} t_{n^0 n}^{LL} \alpha_{lm^0}(\omega; \mathbf{q}^0); \quad (1a)$$

$$u_1^R = \sum_{n^0} t_{n^0 n}^{RL} \alpha_{lm^0}(\omega; \mathbf{q}^0); \quad (1b)$$

where n, n^0, n^0 refer to the different polarized branches of incident, reflected and transmitted waves. Wavevectors for the incident, reflected, and transmitted waves are \mathbf{q}, \mathbf{q}^0 , and \mathbf{q}^0 , respectively. The superscript L and R indicate the left and the right. In these equations, $t_{n^0 n}^{RL}, t_{n^0 n}^{LL}$ are the amplitude transmission/reflection coefficients from mode n on the lead L to mode n^0 on lead R and to mode n^0 on lead L . The wave vectors \mathbf{q}^0 and \mathbf{q}^0 are found to satisfy $\omega = \omega_{n^0}(\mathbf{q}^0) = \omega_{n^0}(\mathbf{q}^0)$ using the generalized eigenvalue decomposition method.¹⁴ Note that frequency does not change because the scattering is elastic. The group velocities v_g for the reflected waves $\alpha_{lm^0}(\omega; \mathbf{q}^0)$ are backward $v_g < 0$, for the transmitted waves $v_g > 0$. In order to obtain the coefficients $t_{n^0 n}^{RL}$ and $t_{n^0 n}^{LL}$, an alternative, but equivalent, form of expression of Eq. (1) has been proposed in Ref. 13 by replacing the summation in Eq. (1) with the operation of matrix multiplication. Eq. (1) can be written in terms of matrix as

$$u_1^L = \alpha_{lm}(\omega; \mathbf{q}) + E(-)_{-1}(\omega) t^0; \quad (2a)$$

$$u_1^R = E(+)_{-1}(\omega) t^0; \quad (2b)$$

Here $E(\pm) = \mathbf{f} e_1; e_2; \dots$ is the matrix formed by the column eigenvectors for the reflected normal modes. $_{-1}(\omega)$ is the diagonal matrix with the diagonal terms ranging from

$e^{iq_1^0 R_1}; e^{iq_2^0 R_1}; \dots; e^{iq_n^0 R_1}$. The column vector t^0 consists of the amplitude reflection coefficients t_{n0}^{LL} with the different indices n^0 . Similar meaning holds for the notations $E(+); t_1(+)$ and t^0 in the right lead, respectively. With the help of Eq. (2), the propagation of the phonon waves^{13,14,15} from l to $l+s$ unit cell can be described by the propagator F^s as $u_{l+s} = F^s u_l$, where $F^s = E_{s+1} E_s^{-1}$. The inverse matrix $E^{(-1)}$ of the matrix E is pseudo-inverse because E is not necessarily a square matrix.

Combining Eq. (2) and the propagator F^s with the equations of motion in the scattering region, we can solve¹⁵ u_1^L and u_1^R in Eq. (1). Then the amplitude transmission/reflection coefficients t^0 and t^0 are gotten through the formulas $t^0 = t_1^1(+)^{-1} E^1(+)^{-1} \tilde{R}$ and $t^0 = t_1^1(-)^{-1} E^1(-)^{-1} \tilde{R}_{lm} u_1^L$. The energy transmission $T_n(!)$ /reflection $R_n(!)$ is related to the amplitude transmission/reflection^{15,19} as $T_n(!) = \frac{P}{P_{n0}} \frac{J_{n0n}^{RL} J_n^2}{J_{n0n}^{LL} J_n^2} \frac{v_n^R}{v_n^L}$ and $R_n(!) = \frac{P}{P_{n0}} \frac{J_{n0n}^{LL} J_n^2}{J_{n0n}^{RL} J_n^2} \frac{v_n^L}{v_n^R}$, respectively, where v^L and v^R are the group velocities for the left and the right.

The achiral carbon nanotube (11;0) with the SW defect is optimized with the second generation Brenner potential.¹⁷ The force constants are derived from the optimized structure under small displacement. The phonon dispersion is calculated using the force constants in the unit cell on the lead. The calculated results are shown in the picture (A) in Fig. 1. We further analyze the symmetrical properties for each normal mode. The achiral zig-zag carbon nanotube (n;0) has the symmetry of the full line group^{1,2} $L_z = T_{2n}^1 D_{nh}$, where T_{2n}^1 is the screw operation and D_{nh} is the point group. However, it is not necessary to work with the full line group. Instead, the point group is sufficient for the analysis of phonon modes because the normal mode vectors at the Γ point ($q = 0$) always transform as irreducible representations of the isogonal point group. The point group isogonal to the line group, i.e. with the same order of the principal rotational axis, is D_{nh} for achiral tubes. The isogonal point group for the zigzag (11;0) CNT is D_{22h} . Each normal mode will form a basis for an irreducible representation of the corresponding line group. The symmetries for normal modes are found by decomposing the representations of symmetrical operation into irreducible representations. The $12n$ branches of phonon modes for the zig-zag (n;0) CNT can be decomposed into the following irreducible representations³ at Γ points

$$\text{zigzag}_{12n} = 2(A_{1g} \quad A_{2u} \quad B_{2g} \quad B_{1u}) \quad A_{2g} \quad B_{1g} \quad A_{1u} \quad B_{2u} \quad \sum_{j=1}^{X-1} 3(E_{jg} \quad E_{ju}): \quad (3)$$

We find that the calculated number of symmetries for (11;0) CNT from the force constants

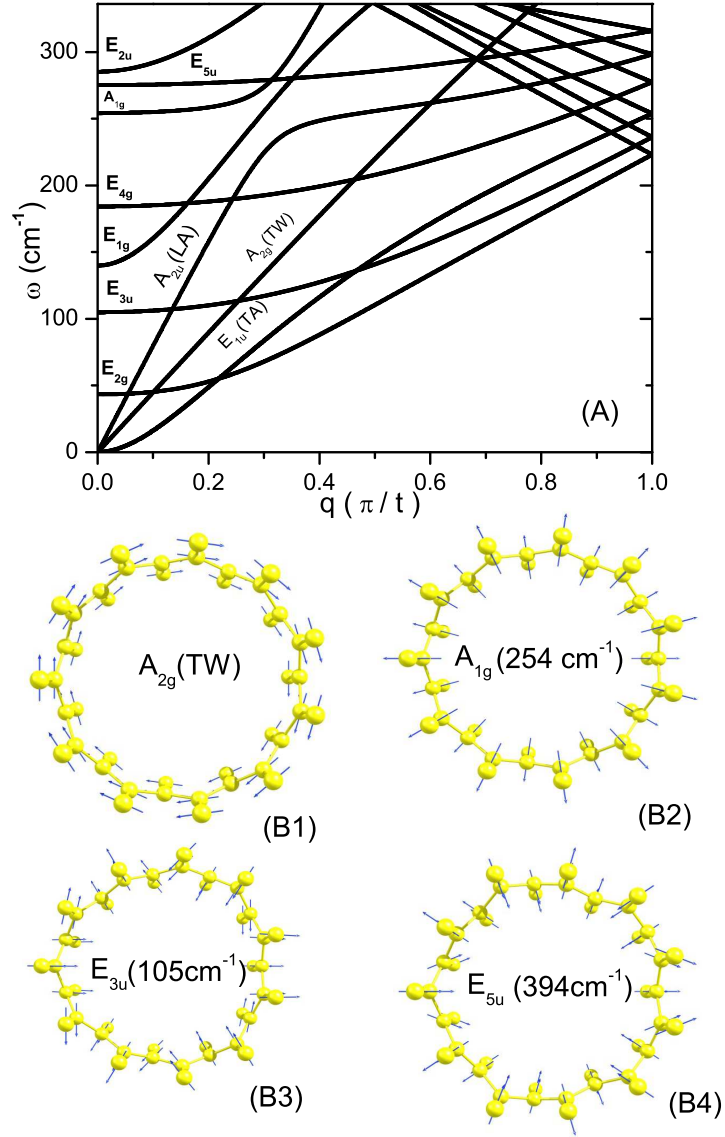


FIG . 1: Phonon dispersion and the symmetry of phonon modes for the achiral (11;0) CNT : (A) Phonon dispersion and the symmetrical notations for each mode at Γ points at low frequency. (B 1)–(B 4) Vibrations of the A_{2g} , A_{1g} , E_{3u} and E_{5u} mode, respectively. Frequency values indicated in the figure are at Γ points.

derived from Brenner potential strictly respect the predicted isogonal D_{22h} symmetry. We list the point group notations at Γ points for the normal modes at low frequency in the picture (A) in Fig. 1. It can be seen from Fig. 1 that symmetry properties for the four acoustic branches are: the longitudinal acoustic mode (LA) ! A_{2u} , the doubly degenerate transverse acoustic mode (TA) ! E_{1u} , and the twist acoustic mode (TW) ! A_{2g} . The

calculated frequency at Γ point for the A_{1g} radial breathing mode (RBM) is 254 cm^{-1} , while the fitted value for RBM mode⁴ is $\omega_{\text{RBM}}(r) = \omega_{(10;10)}(r_{(10;10)}=r)^{1.0017-0.0007} = 260 \text{ cm}^{-1}$. Here $\omega_{(10;10)}$ and $r_{(10;10)}$ are, respectively, the frequency and radius of the (10,10) arm chair CNT, with values of $\omega_{(10;10)} = 165 \text{ cm}^{-1}$ and $r_{(10;10)} = 6.6785 \text{ \AA}$. The calculated RBM frequency agrees with the predicted values. The calculated vibrations for some typical normal modes are plotted in the picture B in Fig. 1. It can be seen that the phonon modes calculated from Brenner potential respect the symmetries of CNTs well.

The calculated single mode phonon transmissions for the LA, TA, and TW acoustic branches are shown in Fig. 2 by the solid lines. The group velocity for each mode is also plotted in Fig. 2 with the dashed lines. It can be seen from Fig. 2 that the transmission for each acoustic branch starts approximately at the value of one near the Γ point, which means that the SW defect CNTs pass long wave acoustic phonons. With the increase of frequency, the group velocity decreases for each acoustic mode. The transmissions for LA, TA, and TW modes reduce in tendency. Especially, a gap in LA mode transmission appears at frequency of $\omega = 250 \text{ cm}^{-1}$, where the corresponding group velocity decreases to a very small value. Compared with that of LA and TA modes, the transmission for TW mode has more rich features. We think that this may be ascribed to the higher symmetry of the atomic vibrations for the TW mode as shown in the picture (B1) in Fig. 1.

The transmissions as a function of frequency for optical modes are shown in Fig. 3. In contrast to the transmission for acoustic modes, the optical mode transmissions have very small values at Γ points because of the low group velocities. This is quite different from the transmission for acoustic modes. The long wave optical phonons are scattered strongly by the SW defect in CNTs. Thus, the optical phonons at Γ points transport less energy in the SW defect CNTs. Optical mode phonons near Γ points contribute more to local heating in the SW defect CNTs. We suggest that this feature can be verified experimentally by measuring the intensities of Raman-active modes such as A_{1g} . With the increase of frequency, the optical mode transmissions increase as shown in Fig. 3. In comparison with the transmission of E_{3u} mode, the transmission for the RBM mode shows more peak features. This can be explained by differences in their symmetrical properties. As shown in the picture (B2), (B3) and (B4) in Fig. 1, the vibrations of A_{1g} mode have higher symmetry than those of E_{3u} mode while the vibrations of the E_{3u} and E_{5u} modes seem to distort the symmetrical structure of CNTs. Therefore, the transmission for the A_{1g} mode is more sensitive to the SW

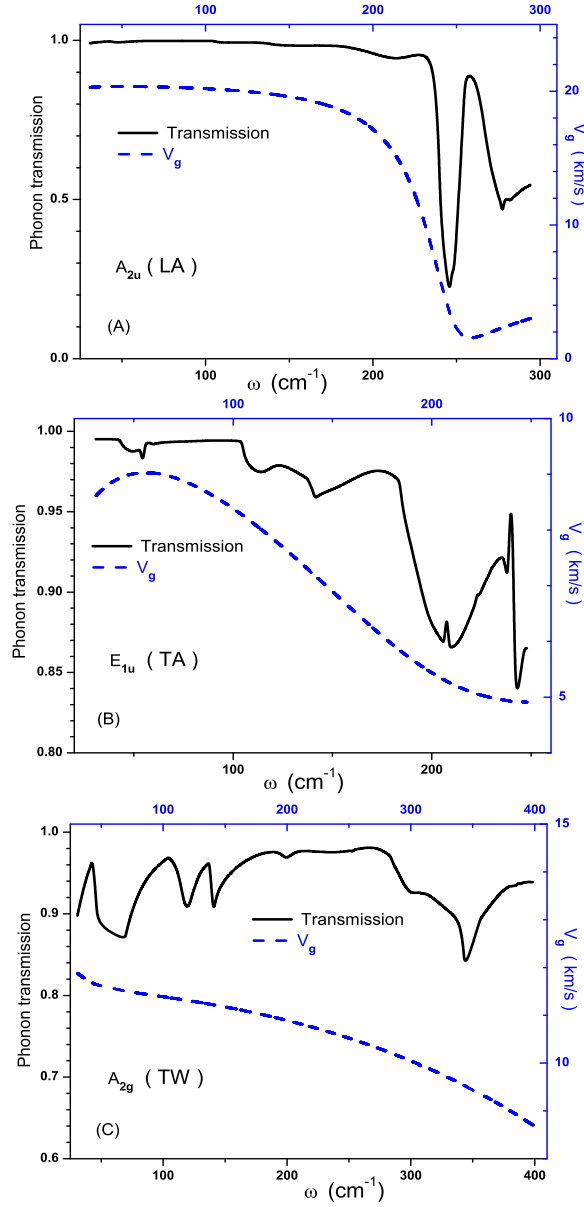


FIG. 2: Frequency dependence of phonon transmissions and group velocities for acoustic modes: (A) LA mode with the symmetry of A_{2u} ; (B) TA mode with the symmetry of E_{1u} ; (C) TW mode with the symmetry of A_{2g} .

defect in CNTs, which breaks the symmetry. Together with the transmission features for the acoustic phonons with higher symmetry such as the TW mode, it can be inferred that the transmissions both for the acoustic and optical phonons with high symmetrical properties are sensitive to the symmetry breaking. This symmetrically mode-dependent behavior for the single mode phonon transmission may help to distinguish the different phonon modes

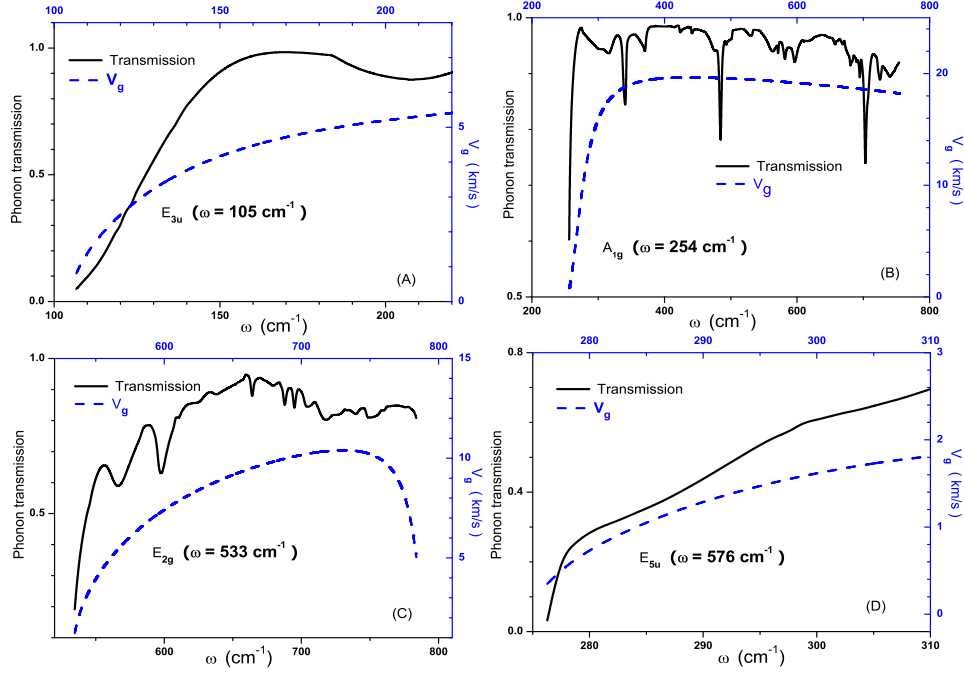


FIG. 3: Frequency dependence of phonon transmissions and group velocities for optical modes:

(A) E_{3u} mode with $\omega = 105 \text{ cm}^{-1}$ at Γ point; (B) A_{1g} mode with $\omega = 254 \text{ cm}^{-1}$ at Γ point; (C) E_{2g} mode with $\omega = 533 \text{ cm}^{-1}$ at Γ point; (D) E_{5u} mode with $\omega = 576 \text{ cm}^{-1}$ at Γ point.

through their transport features after the symmetry breaking.

In summary, the single-mode phonon transmissions are calculated for the symmetry broken CNT (11;0) in the presence of the SW defect using the mode-matching method. The symmetries of normal mode phonons are analyzed in comparison with the phonon transmissions. It is found that the acoustic phonon transmissions decrease with the reduced group velocity at high frequencies while the optical phonon transmissions have very small values near Γ points. The features of single-mode phonon transmission after symmetry breaking are related to the symmetry property of each normal mode. These findings may help to reveal the local heating problem in the defect CNTs. No evident mode conversion has been observed during our calculation. We also calculated other different chirality CNTs in the presence of the SW defect and similar findings can be made. Our present calculation holds at moderately low temperature where anharmonic scattering does not play an important role. When temperature is sufficiently high, nonlinear scattering should be considered.

We thanks Lu Jingtao and Yang Huijie for helpful discussions. This work was supported

in part by a Faculty Research Grant (R-144-000-173-101/112) of National University of Singapore. J. Wang thanks National Natural Science Foundation of China (NSFC) under the grant 10705023.

-
- ¹ M. Damjanovic, I. Milosevic, T. Vukovic and R. Sredanovic, Phys. Rev. B 60, 2728 (1999).
 - ² S. Reich, C. Thomsen, J. Maultzsch, Carbon Nanotubes: Basic Concepts and Physical Properties, WILEY-VCH, 2004.
 - ³ O. E. Alon, Phys. Rev. B 63, 201403 (2001).
 - ⁴ R. Saito, G. Dresselhaus, and M. S. Dresselhaus, Physical Properties of Carbon Nanotubes, Imperial College Press, 1998.
 - ⁵ M. S. Dresselhaus, G. Dresselhaus, P. Avouris, (Eds.), Carbon Nanotubes: Synthesis, Structure, Properties and Application, Topics Appl. Phys. 80 (2001).
 - ⁶ P. Kim, L. Shi, A. Majumdar, and P. L. McEuen, Phys. Rev. Lett. 87, 215502 (2001).
 - ⁷ H.-Y. Chiu, V. V. Deshpande, H. W. Ch. Postma, C. N. Lau, C. Miko, L. Forro, and M. Bockrath, Phys. Rev. Lett. 95, 226101 (2005).
 - ⁸ P. W. Anderson, Science, 177, 393 (1972).
 - ⁹ T. Yamamoto and K. Watanabe, Phys. Rev. Lett. 96, 255503 (2006).
 - ¹⁰ M. Terraneo, M. Peyrard, and G. Casati, Phys. Rev. Lett. 88, 094302 (2002).
 - ¹¹ C. W. Chang, D. Okawa, A. Majumdar, A. Zettl, Science 314, 1121 (2006).
 - ¹² L. Wang and B. Li, Phys. Rev. Lett. 99, 177208 (2007).
 - ¹³ T. Ando, Phys. Rev. B 44, 8017 (1991).
 - ¹⁴ P. A. Khomyakov, G. Brocks, Phys. Rev. B 70, 195402 (2004).
 - ¹⁵ J.-S. Wang, J. Wang, and J. T. Lu, Eur. Phys. J. B 62, 381 (2008).
 - ¹⁶ J.-S. Wang, J. Wang, N. Zeng, Phys. Rev. B 74, 033408 (2006).
 - ¹⁷ D. Brenner, O. Shenderova, J. Harrison, S. Stuart, B. Ni, and S. Sinnott, J. Phys.: Condens. Matter. 14, 783 (2002).
 - ¹⁸ N. Mingo, D. A. Stewart, D. A. Broido, and D. Srivastava, Phys. Rev. B 77, 033418 (2008).
 - ¹⁹ J. Wang, J.-S. Wang, Phys. Rev. B 74, 054303 (2006).